49th AIAA Aerospace Sciences Meeting including the New Horizons Forum and Aerospace Exposition
4 - 7 January 2011, Orlando, Florida

AIAA 2011-657

Analysis and correction of errors generated by slowly moving shocks

Eric Johnsen *
University of Michigan, Ann Arbor, MI 48109, USA
Sanjiva K. Lele† and Johan Larsson ‡
Stanford University, Stanford, CA 93405, USA

In problems where shock waves move slowly relative to the grid, numerical errors in density and momentum may occur at the shock and propagate downstream, thereby contaminating the solution. These errors are analyzed in the present work and a fix is proposed. The errors are divided into two classes: *start-up* errors and *post-shock oscillations*. It is shown that a traveling wave analysis of the isothermal Euler equations describes the spike formation in the momentum for the first-order accurate Lax-Friedrichs solver very well. By smearing the density and momentum profiles appropriately, the corresponding downstream-propagating wave can be removed. The post-shock oscillations have been characterized; as a fix for this problem, a lower bound on the wave speed of the first-order accurate HLL solver is set in the artificial viscosity coefficient for density in the continuity equation. The implementation to higher-order accurate methods is not straightforward; an additional fix is proposed, which is performs well on the full multi-dimensional Euler equations.

I. Introduction

If shock waves are not treated accurately in computational fluid dynamics applications, numerical errors may propagate in the flow field and contaminate the solution. Because of its simplicity and robustness, shock capturing has become over the past decades the most common means for simulating flows with shock waves in a stable fashion. Shock-capturing schemes are based on the premise that, because shocks are discontinuous structures (or very thin regions) that cannot be resolved on the computational grid, numerical dissipation is introduced to stabilize the solution. Thus, shocks are in practice smeared over a few computational cells. An important drawback of many commonly used shock-capturing schemes is that numerical errors are generated in computations of slowly-moving shocks. For shocks moving slowly relative to the grid, errors and oscillations in density and momentum may occur at the shock and propagate downstream, thereby contaminating the solution, depending on the numerical scheme. Although the occurrence of errors generated by slowly-moving shocks has been observed for many years,[10,12] few systematic studies of the phenomenon exist. This problem is of particular importance in flows in which the errors are on the order of small fluid fluctuations, *e.g.*, in noise generation, acoustics and turbulence.

Post-shock oscillations were first identified in simulations of a Mach 3 flow over a step.[18] It was further argued that the dissipation introduced by Godunov's method vanishes as the shock speed goes to zero,[2] so that the entropy production across the shock is incorrect. The introduction of additional dissipation is proposed as a fix. The first systematic study[13] showed that errors at slowly-moving shocks occur only in nonlinear systems of equations and that the amplitude of the oscillations depended on the numerical method. Furthermore, it was shown that oscillations are shed at a period, $\lambda_s \Delta x/s$, where λ_s is the characteristic speed of the shock family and s is the shock speed. A quantification of the error and a modified entropy fix were provided,[11] though results still showed some oscillations. Along the same lines, entropy fixes have been

*Assistant Professor, Mechanical Engineering Department, AIAA Member.
†Professor, Aeronautics and Astronautics Department, AIAA Member.
‡Research Associate, Center for Turbulence Research, AIAA Member.

developped to correct such spurious oscillations.[8,16] The characteristic variables can be visualized in state space to show that intermediate states (*i.e.*, points in the smeared shock profile) lie on the non-physical branch of the Hugoniot locus connecting the states upstream and downstream of the shock.[1] An important advance in understanding errors related to slowly-moving shocks was made[6] when it was realized that the smeared density profile introduces a spike in the momentum at the shock location. Thus, downstream-propagating waves are generated to balance the momentum. Furthermore, it was shown that these problems are in fact accentuated when using higher-order accurate schemes.

The objective of the present work is to provide a more comprehensive understanding of errors generated by slowly-moving shocks. Thus, for practical purposes, the flow regimes for which this issue is likely to be detrimental can be determined. Two types of errors generated by slowly-moving shocks are first classified; then, a modification to existing solvers is presented to prevent certain errors. Thereafter, a fix for higher-order accurate methods is proposed. Finally, examples for the two-dimensional Euler equations are presented.

II. Governing equations

For simplicity, the present analysis focuses on the one-dimensional isothermal Euler equations; the results will subsequently be extended to the full Euler equations. If the temperature is assumed constant, the sound speed, a, is constant, and $dp = a^2 d\rho$, where p is the pressure and ρ is the density. As a result, the Euler equations become:[17]

$$\mathbf{q}_t + \mathbf{f}(\mathbf{q})_x = \mathbf{0}, \quad \mathbf{q} = \begin{pmatrix} \rho \\ \rho u \end{pmatrix}, \quad \mathbf{f} = \begin{pmatrix} \rho u \\ \rho u^2 + \rho a^2 \end{pmatrix}, \tag{1}$$

where u is the velocity. The eigenvalues and right eigenvectors of the flux Jacobian are

$$\lambda^{(1)} = u - a, \quad \lambda^{(2)} = u + a, \qquad \mathbf{r}^{(1)} = \begin{pmatrix} 1 \\ u - a \end{pmatrix}, \quad \mathbf{r}^{(2)} = \begin{pmatrix} 1 \\ u + a \end{pmatrix}. \tag{2}$$

Without loss of generality, consider a right-moving shock ($s > 0$) with compression (*i.e.*, density gradient) pointing in the negative x direction. The state ahead of the shock is the right state and that behind the shock is the left state. The isothermal Euler equations can be integrated over a fixed control volume enclosing the shock to yield normal shock relations. The velocity can then be expressed as

$$u_L = u_R + a\sqrt{\frac{\rho_R}{\rho_L}}\left(\frac{\rho_L}{\rho_R} - 1\right), \tag{3}$$

and the shock velocity by

$$s = u_R + a\sqrt{\frac{\rho_L}{\rho_R}}, \tag{4}$$

where $M = \sqrt{\rho_L/\rho_R}$ is the shock Mach number. Thus, given M and ρ_R and choosing s,

$$u_R = s - aM, \qquad \rho_L = \rho_R M^2, \qquad u_L = u_R + a\left(M - \frac{1}{M}\right). \tag{5}$$

For the present work, base values of $M = 2$ (unless otherwise mentioned) and $\rho_R = 1$ are selected and s is varied; the remaining quantities are computed to satisfy Equations 5.

Given the relations in Equations 5, it can be shown that the eigenvalues depend only on s and M. The first eigenvalue can be written:

$$\lambda_L^{(1)} = u_L - a = s - a\left(1 + \frac{1}{M}\right), \qquad \lambda_R^{(1)} = u_R - a = s - a(M+1). \tag{6}$$

For the present case, s is small and positive, so that $\lambda_L^{(1)}$ and $\lambda_R^{(1)}$ are both negative. The second eigenvalue can be written:

$$\lambda_L^{(2)} = u_L + a = s + a\left(1 - \frac{1}{M}\right), \qquad \lambda_R^{(2)} = u_R + a = s - a(M-1). \tag{7}$$

Thus, $\lambda_L^{(2)} > 0$ always, but $\lambda_R^{(2)}$ may be negative if

$$u_R < -a \quad \text{or} \quad s < a(M-1). \tag{8}$$

III. Riemann solvers

To simplify the analysis, a first-order accurate spatial discretization is first considered. The time-marching is handled by a third-order accurate TVD Runge-Kutta scheme.[3] The semi-discrete form of the equations is given by:

$$\frac{d}{dt}\begin{pmatrix} \bar{\rho}_i \\ \overline{\rho u}_i \end{pmatrix} = \frac{1}{\Delta x}\begin{pmatrix} \rho u_{i+1/2} - \rho u_{i-1/2} \\ (\rho u^2 + \rho a^2)_{i+1/2} - (\rho u^2 + \rho a^2)_{i-1/2} \end{pmatrix}, \tag{9}$$

where the bar denotes the cell-average value. Four different approximate Riemann solvers are considered: Lax-Friedrichs, Rusanov, Roe and HLL. All of the schemes under consideration can be written as a central term plus a diffusive term, whose viscosity may vary but which goes to zero as the grid is refined, *i.e.*,

$$\rho u_{i+1/2} = \frac{\rho u_i + \rho u_{i+1}}{2} - c^{(\rho)}_{i+1/2}(\rho_{i+1} - \rho_i) - c^{(\rho u)}_{i+1/2}(\rho u_{i+1} - \rho u_i), \tag{10}$$

$$\rho u^2 + \rho a^2_{i+1/2} = \frac{(\rho u^2 + \rho a^2)_i + (\rho u^2 + \rho a^2)_{i+1}}{2} - m^{(\rho)}_{i+1/2}(\rho_{i+1} - \rho_i) - m^{(\rho u)}_{i+1/2}(\rho u_{i+1} - \rho u_i), \tag{11}$$

where c and m are the numerical viscosity coefficients. The diffusive term can be written more concisely in matrix form:

$$\begin{pmatrix} c^{(\rho)}_{i+1/2} & c^{(\rho u)}_{i+1/2} \\ m^{(\rho)}_{i+1/2} & m^{(\rho u)}_{i+1/2} \end{pmatrix}\begin{pmatrix} \rho_{i+1} - \rho_i \\ \rho u_{i+1} - \rho u_i \end{pmatrix}. \tag{12}$$

The Lax-Friedrichs (LF) and Rusanov (Local Lax-Friedrichs or LLF) fluxes are defined as:[9,15]

$$f_{i+1/2} = \frac{1}{2}(f_i + f_{i+1}) - \frac{\beta_{i+1/2}}{2}(q_{i+1} - q_i). \tag{13}$$

For the Lax-Friedrichs scheme, β is a global value (*i.e.*, the largest eigenvalue over the whole domain):

$$\beta_{i+1/2} = \max_{i,p} |\lambda^{(p)}_i|. \tag{14}$$

For the Rusanov scheme, a local value of β is utilized:

$$\beta_{i+1/2} = \max_{p}(|\lambda^{(p)}_i|, |\lambda^{(p)}_{i+1}|). \tag{15}$$

For the LF or LLF solvers, the artificial viscosity coefficients can then be written:

$$c^{(\rho)}_{i+1/2} = \beta_{i+1/2}/2, \qquad c^{(\rho u)}_{i+1/2} = 0, \qquad m^{(\rho)}_{i+1/2} = 0, \qquad m^{(\rho u)}_{i+1/2} = \beta_{i+1/2}/2. \tag{16}$$

The Roe flux is defined as:[14]

$$f_{i+1/2} = \frac{1}{2}(f_i + f_{i+1}) - \frac{1}{2}\sum_p \tilde{\alpha}^{(p)}_{i+1/2}|\tilde{\lambda}^{(p)}_{i+1/2}|\tilde{r}^{(p)}_{i+1/2}. \tag{17}$$

Here, the tilde denotes Roe-averaged quantities. For the isothermal Euler equations, only the velocity is needed:

$$\tilde{u}_{i+1/2} = \frac{\sqrt{\frac{\rho_i}{\rho_{i+1}}}u_i + u_{i+1}}{\sqrt{\frac{\rho_i}{\rho_{i+1}}} + 1}. \tag{18}$$

For the Roe solver, the artificial viscosity coefficients can then be written:

$$c^{(\rho)}_{i+1/2} = \frac{|\tilde{\lambda}^{(1)}_{i+1/2}|\tilde{\lambda}^{(2)}_{i+1/2} - |\tilde{\lambda}^{(2)}_{i+1/2}|\tilde{\lambda}^{(1)}_{i+1/2}}{4a}, \qquad c^{(\rho u)}_{i+1/2} = \frac{|\tilde{\lambda}^{(2)}_{i+1/2}| - |\tilde{\lambda}^{(1)}_{i+1/2}|}{4a}, \tag{19}$$

$$m^{(\rho)}_{i+1/2} = -\tilde{\lambda}^{(1)}_{i+1/2}\tilde{\lambda}^{(2)}_{i+1/2}c^{(\rho u)}_{i+1/2}, \qquad m^{(\rho u)}_{i+1/2} = c^{(\rho)}_{i+1/2} + (\tilde{\lambda}^{(1)}_{i+1/2} + \tilde{\lambda}^{(2)}_{i+1/2})c^{(\rho u)}_{i+1/2}. \tag{20}$$

The Harten-Lax-van Leer (HLL) flux is defined as:[4]

$$f_{i+1/2} = \frac{s^+_{i+1/2} f_i - s^-_{i+1/2} f_{i+1} + s^+_{i+1/2} s^-_{i+1/2} (q_{i+1} - q_i)}{s^+_{i+1/2} - s^-_{i+1/2}}, \tag{21}$$

where the wave speeds are given by

$$s^-_{i+1/2} = \min(0, \lambda^{(1)}_i, \tilde{\lambda}^{(1)}_i), \quad s^+_{i+1/2} = \max(0, \lambda^{(2)}_{i+1}, \tilde{\lambda}^{(2)}_{i+1}). \tag{22}$$

For the HLL solver, the artificial viscosity coefficients can then be written:

$$c^{(\rho)}_{i+1/2} = \frac{-s^-_{i+1/2} s^+_{i+1/2}}{s^+_{i+1/2} - s^-_{i+1/2}}, \qquad c^{(\rho u)}_{i+1/2} = \frac{1}{2} \frac{s^+_{i+1/2} + s^-_{i+1/2}}{s^+_{i+1/2} - s^-_{i+1/2}}, \tag{23}$$

$$m^{(\rho)}_{i+1/2} = -\tilde{\lambda}^{(1)}_{i+1/2} \tilde{\lambda}^{(2)}_{i+1/2} c^{(\rho u)}_{i+1/2}, \qquad m^{(\rho u)}_{i+1/2} = c^{(\rho)}_{i+1/2} + (\tilde{\lambda}^{(1)}_{i+1/2} + \tilde{\lambda}^{(2)}_{i+1/2}) c^{(\rho u)}_{i+1/2}, \tag{24}$$

where the tilde denote Roe-averaged quantities. The following property of Roe averages was used:

$$\Delta(\rho u^2) = \Delta((\rho u)^2/\rho) = 2\tilde{u}\Delta(\rho u) - \tilde{u}^2 \Delta\rho. \tag{25}$$

In the LF and Rusanov solvers, the artificial diffusivity coefficients matrix is diagonal with positive non-zero entries. In the Roe and HLL solvers, this is not necessarily the case. The first two schemes are essentially artificial diffusion methods in which an explicit diffusive term is added, while the latter two methods are based on upwinding, in which the direction of the eigenvalues gives the direction of the wind. As illustrated by the results in the following sections, the Roe and HLL solvers are in fact almost identical for the isothermal Euler equations. Even though the development of the Roe and HLL solvers is different, their artificial viscosity coefficients are very similar, as observed in Equations 19 and 23. The main difference resides in the coefficients of the continuity equation.

IV. Classification and characterization of the errors

In order to illustrate the types of errors that are generated by shocks that move slowly with respect to the grid, Figure 1 shows time series of the propagation of a shock moving at speed, $s = 0.1$ (with $M = 2$). The LF, Rusanov, Roe and HLL solvers are all included on plots of density, momentum and the characteristic variables ($C^{\pm}$). Different solvers lead to different behaviors, although the HLL solver matches the Roe solution almost identically, as expected. Initially, an undershoot (or *spike*[6]) develops in the momentum in all solvers and propagates with the shock. By conservation, an excess of momentum propagates downstream of the shocks, along the C^- characteristic. As a result, a deficit of mass propagates downstream of the shock as well. Interestingly, there are no significant errors in the C^+ characteristic variable. After this initial disturbance, the solution is very different, depending on the family of solvers. In the LF and Rusanov cases, the shock takes a viscous profile and propagates to the right; the momentum spike persists, such that the shock appears to adopt a steady-state profile. In the Roe and HLL cases, the momentum spike oscillates in an unsteady fashion, thereby leading to the propagation of oscillations downstream of the shock. These oscillations tend to die out as they propagate away from the shock, due to the dissipative nature of these first-order accurate schemes. The momentum profiles offer the most evident depiction of these errors and will be used throughout the rest of the article.

In light of the the present observations and past work[6,8] in which different classes of solvers were considered, the errors generated by slowly-moving shocks may be divided into two types:

1. *Start-up errors*: these errors refer to the initially generated error that consists of a spike in the momentum moving with the shock and an excess of momentum (and mass) propagating downstream of the shock. In this case, the shock profile reaches a steady state. This error applies to all the solvers under consideration and seems the most substantial for the LF and Rusanov solvers.

2. *Post-shock oscillations*: these errors refer to oscillations that are generated in a periodic fashion. As the momentum spike grows and shrinks, oscillations are generated downstream of the shock. In this case, the shock profile is unsteady. This error only applies to the Roe and HLL solvers.

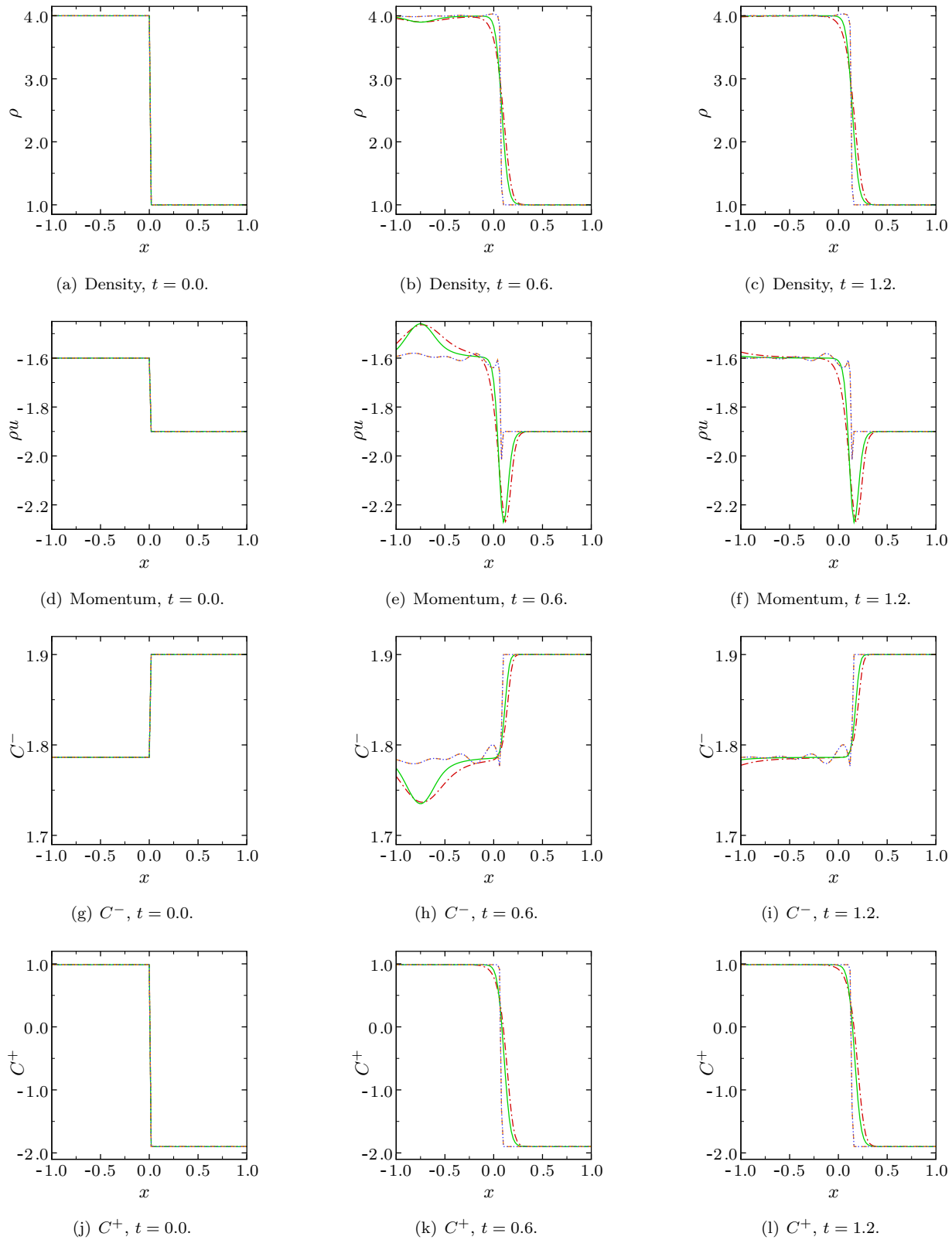

(a) Density, $t = 0.0$. (b) Density, $t = 0.6$. (c) Density, $t = 1.2$.

(d) Momentum, $t = 0.0$. (e) Momentum, $t = 0.6$. (f) Momentum, $t = 1.2$.

(g) C^-, $t = 0.0$. (h) C^-, $t = 0.6$. (i) C^-, $t = 1.2$.

(j) C^+, $t = 0.0$. (k) C^+, $t = 0.6$. (l) C^+, $t = 1.2$.

Figure 1. Mach 2 shock moving at speed $s = 0.1$ with the LF (red dashed-dot), Rusanov (green solid), Roe (orange dashed) and HLL (blue dotted) solvers.

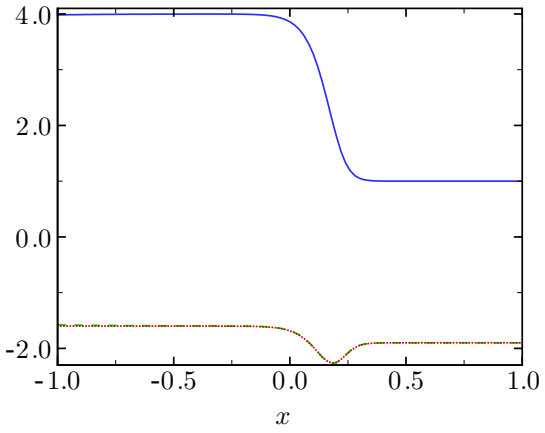

(a) Density (blue solid), momentum (green dashed) and traveling wave solution of momentum (red dotted) at $t = 1.2$.

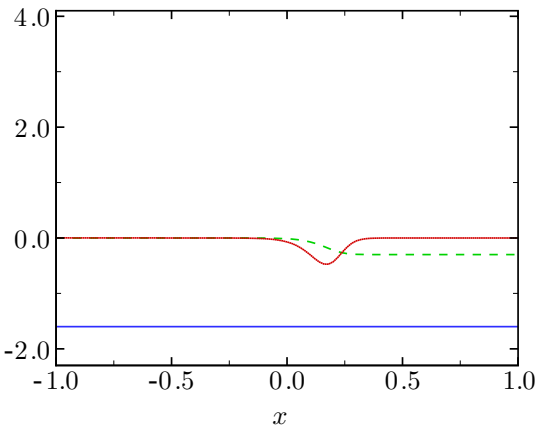

(b) ρu_L (blue solid), $s(\rho - \rho_L)$ (green dashed), and $\epsilon\rho'$ (red dotted) at $t = 1.2$.

Figure 2. Traveling wave solution and computed solutions for $s = 0.1$.

V. Analysis and correction of start-up errors

The generation of the momentum spike is attributed to the smeared density profile.[6] Following a traveling wave analysis, the momentum can be expressed based on the velocity:

$$\rho u = \rho u_L + s(\rho - \rho_L) + \epsilon\rho', \tag{26}$$

where L denotes the state on the left of the shock (at infinity), the prime denotes differentiation with respect to the variable, $\xi = x - st$, and ϵ is the viscosity introduced in the traveling wave analysis. The momentum consists of the superposition of a constant term, ρu_L, a monotone diffuse profile, $s(\rho - \rho_L)$, and a spike, $\epsilon\rho'$. Thus, the prominence of the spike depends on the relative magnitude of $s\rho$ and $\epsilon\rho'$.

To understand the dependence of the spike amplitude on the shock speed, the traveling wave analysis can be directly applied in the case of the LF solver. Then, $\epsilon = \beta\Delta x/2$, where $\beta = |\lambda_R^{(1)}| = 2.9$. As an example, $\Delta x = 0.02$ is taken, and shocks speed of $s = 0.1$ (with $\beta = 2.9$, $\epsilon = 0.029$) and $s = 0.4$ (with $\beta = 2.6$, $\epsilon = 0.026$) are considered. Figure 2 shows the density and momentum from the simulations for $s = 0.1$ at time $t_f = 1.2$ and the momentum calculated from Equation 26 based on the density profile. In addition, the contribution of each of the three terms on the right-hand side of Equation 26 is plotted. The traveling wave solution calculated from Equation 26 using the density profile from the simulations matches the computed momentum profile, as expected. The only discrepancies are due to the initial downstream-propagating wave, which compensates for the formation of the momentum spike. However, after some time, the profiles adopt a steady-state solution. Clearly, the amplitude of the spike depends on the shock speed. Though ϵ depends on the shock speed through Equations 6 and 7, the dependence of that term on s in Equation 26 is not very strong, such that the prominence of the spike is mainly governed by s. Hence, the term $\epsilon\rho'$ does not change considerably with s; the most significant term is $s(\rho - \rho_L)$. This analysis shows that shocks for which s is not small do not exhibit a large momentum spike.

It can be concluded that the momentum spike cannot be avoided because of the (artificially) viscous shock profile.[6] However, the downstream-propagating wave that compensates for the spike formation does interact with any flow structures downstream of the shock. This error can be corrected by simply initializing the shock profile to an appropriate traveling wave solution. Assuming that, once the shock adopts a diffuse profile, density is convected at the shock velocity and diffuses with artificial viscosity, ϵ, then

$$\rho(x) = \rho_1 \frac{1 - \mathrm{erf}(\eta)}{2} + \rho_2 \frac{1 + \mathrm{erf}(\eta)}{2}, \quad \eta = \frac{x}{2\sqrt{\epsilon}\sqrt{c\Delta x}}, \tag{27}$$

where c is some empirically-determined constant, which is expected to depend on the spatial scheme (solver, order of accuracy), but not on Δx. The momentum can then be determined from Equation 26. In the case

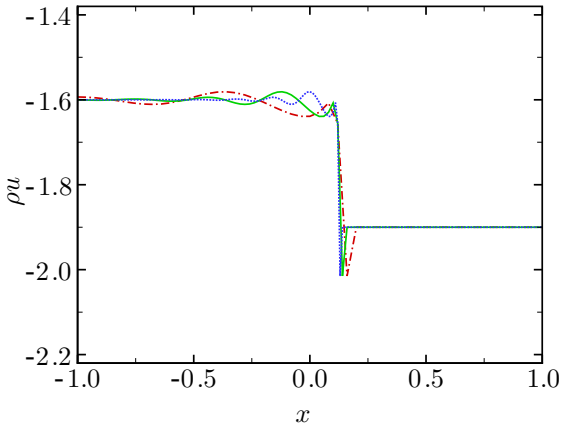

(a) Momentum profiles for $\Delta x = 0.04$ (red dashed-dotted), $\Delta x = 0.02$ (green solid), and $\Delta x = 0.01$ (blue dotted) at $t = 1.2$.

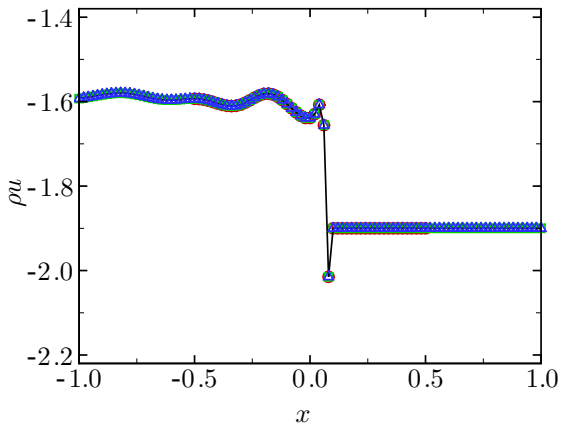

(b) Momentum profiles for $\Delta x = 0.04$ at $t = 1.2$ on a grid stretched by a factor of 2 (red circles), $\Delta x = 0.02$ at $t = 0.6$ (green squares), and $\Delta x = 0.01$ at $t = 0.3$ on a grid stretched by a factor of 2 (blue triangles).

Figure 3. Momentum profiles for $s = 0.1$, using the Roe solver.

of the Lax-Friedrichs solver, $\epsilon = \max_{i,p} |\lambda^{(p)}|$. The traveling wave profiles depend on the coefficient, c. For a value of $c \approx 5$, the smallest error is achieved ($\sim 5\%$ of the momentum jump, compared to 25% and 60%). In practice, an initial error is generated because the density does not exactly obey the proposed diffuse profile.

The present work shows that initially smearing shocks in an arbitrary fashion may lead to the generation of a spurious wave that propagates downstream of the shock. Thus, when initializing the shock as a smooth profile, the procedure should follow the traveling wave solution to prevent the downstream-propagating wave to be generated.

VI. Analysis and correction of post-shock oscillations

As observed previously, post-shock oscillations are generated as the shock propagates through the grid when using the Roe and HLL solvers. The wavelength associated with the error is $\lambda \Delta x / s$, where λ is the eigenvalue not associated with the shock family.[13] In other words, an overshoot/undershoot is generated every time the shock traverses a cell. This phenomenon is repeatable, as illustrated in Figure 3, which shows momentum profiles for grid spacings, $\Delta x = 0.04, 0.02, 0.01$, keeping the CFL constant. In the first plot, the solution is shown at time $t = 1.2$, while in the second plot the solution is shown at times $t = 1.2, 0.6, 0.3$, on a grid stretched by factors of $0.5, 1.0, 2.0$, respectively. The frequency of post-shock oscillations increases as the grid is refined, as expected. However, the amplitude of the oscillations does not decrease with N. This behavior motivates the need for a better understanding of the problem.

As illustrated in Section IV, post-shock oscillations do not occur when using the LF and Rusanov solvers, while the Roe and HLL solvers clearly exhibit such errors. There are two main differences between the Roe/HLL and LF/Rusanov solvers: the artificial viscosity coefficients in the Roe/HLL solvers are not always positive, and in both the continuity and momentum equations, the numerical diffusion is based on both conservative variables. For initial conditions for a $M = 2$ shock, Figure 4 shows the initial artificial viscosity coefficients of density and momentum in both the continuity and momentum equations; the left, Roe-averaged and right states are plotted. It is clear that certain coefficients are negative, such that the relevant term is in fact anti-diffusive.

In the case of a slowly moving shock, the right-propagating wave in the HLL solver $s^+ = 0$ ahead of the shock, so that $c^{(\rho)} = 0$ and $c^{(\rho u)} = -1/2$, so that $m^{(\rho)} > 0$ and $m^{(\rho u)} > 0$. The quantity, $s^+ = 0$, is expected to lead to problems since $c^{(\rho)} = 0$ and $c^{(\rho u)} < 0$, so this quantity is varied in the viscosity coefficients. Figure 5 shows momentum profiles for different global values of s^+ and compares the optimal global value with a local scheme. A value of $s^+ = 0$ corresponds to the original HLL solver for this problem. It can be observed that large values of s^+ exhibit more dissipative features, particularly at the spike. Decreasing the value of s^+ reduces the dissipation, but the cost for this is the presence of post-shock oscillations. The value of s^+

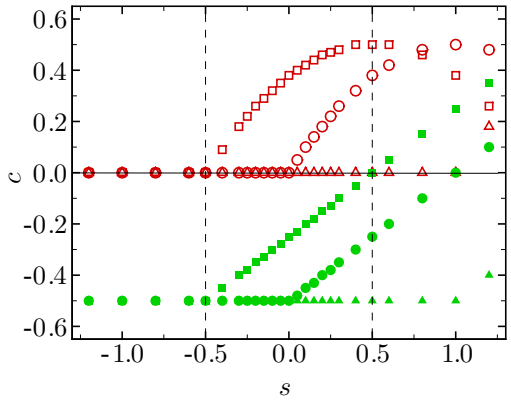

(a) Artificial viscosity coefficents for the density in the continuity equation (open square: $c_L^{(\rho)}$; open circle: $\tilde{c}^{(\rho)}$; open triangle: $c_R^{(\rho)}$) and momentum equation (filled square: $c_L^{(\rho u)}$; filled square: $\tilde{c}^{(\rho u)}$; filled square: $c_R^{(\rho u)}$).

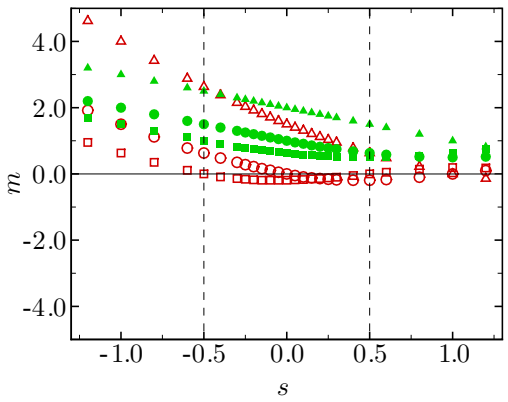

(b) Artificial viscosity coefficents for the momentum in the continuity equation (open square: $m_L^{(\rho)}$; open circle: $\tilde{m}^{(\rho)}$; open triangle: $m_R^{(\rho)}$) and momentum equation (filled square: $m_L^{(\rho u)}$; filled square: $\tilde{m}^{(\rho u)}$; filled square: $m_R^{(\rho u)}$).

Figure 4. Initial artificial viscosity coefficients as a function of the shock speed for $M = 2$. Red open symbols: coefficients for the continuity equation; green filled symbols: coefficients for the momentum equation.

that exhibits the least amount of dissipation, while preventing downstream oscillations, is $s^+ = 0.6 = \lambda_L^{(2)}$. In order to reduce the dissipation further, a localized version can be used; such a formulation is necessary when more complex problems are considered. It is noticed that such a fix is required near the shock and only when $\lambda_i^{(2)}\lambda_{i+1}^{(2)} < 0$. Since shocks are typically spread over approximately five cells, the value of $s^+ = \lambda_L^{(2)}$ is set only when:

$$\lambda_j^{(2)}\lambda_{j+1}^{(2)} < 0, \quad j \in [i-2, i+2]. \tag{28}$$

Though not shown here explicitly, it is noted that a bound on the wave speed in the artifical diffusion of density in the continuity equation only is sufficient to prevent oscillations. Thus, the fix is applied in this field only.

For practical applications, it is of interest to know the range of s over which the errors due to slowly moving shocks are expected to affect the flow. For simplicity, the errors are computed after the initial transient has occurred. The error is normalized by the jump in the relevant quantity, as follows:

$$\Delta f = \frac{f_{exact} - f_{computed,max}}{|f_L - f_R|}. \tag{29}$$

Thus, a positive value implies an undershoot and a negative value implies an overshoot. Figure 6 shows the overshoot in density, the overshoot in momentum downstream of the shock and the undershoot of the spike as a function of the shock speed for $M = 2$. The Roe solver, the Roe solver with Karni's entropy fix[8] (Roe-fix), and the present HLL fix are included. The error in density is not very large in general for this shock strength (up to 1%). The Roe-fix[8] works well, and the present fix even better. Though not shown here, the errors increase with increasing M. As an example, the errors with the Roe-fix[8] become larger for $M = 4$, while with the present fix the error still remains negligible. Similar findings are observed in the momentum overshoot, but in which the error without the fixes can reach 30%. As mentioned in the previous sections, the occurrence of the spike cannot be avoided unless the initial conditions are regularized. For small shock speeds, this error can be extremely large (up to 300%) for all three solvers.

VII. Extension to higher-order accuracy

Higher-order accurate schemes, such as weighted essentially non-oscillatory (WENO) schemes,[5] exhibit severe post-shock oscillations in problems with slowly moving shocks, even with the Lax-Friedrichs solver.[6] For such methods, the problem is even more serious than for low-order accurate methods, as the errors are

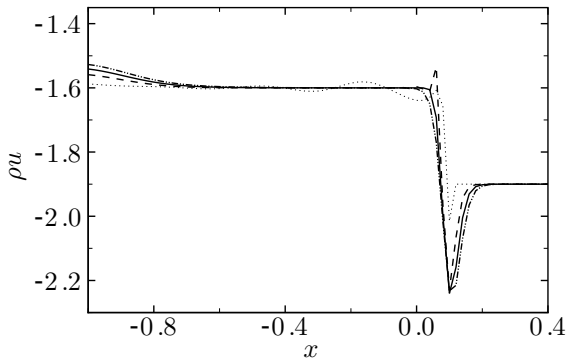

(a) Different values of s^+. Dotted: 0.1; dashed: 0.4, solid: 0.6, dash-dotted: 0.8.

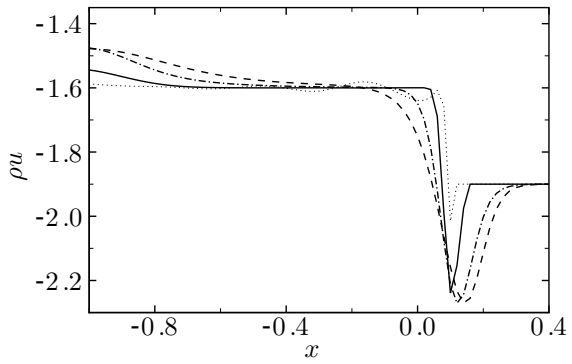

(b) Different solvers. Dotted: Roe; dashed: Lax-Friedrichs; solid: HLL with fix; dash-dotted: Rusanov.

Figure 5. Momentum profiles for the HLL fix with $s = 0.1$.

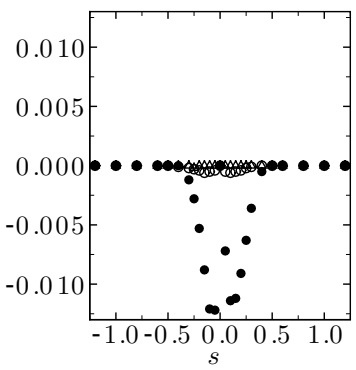

(a) Error in density

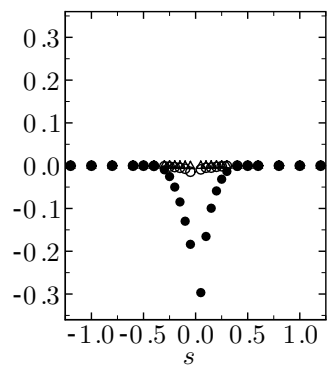

(b) Error in the overshoot of momentum

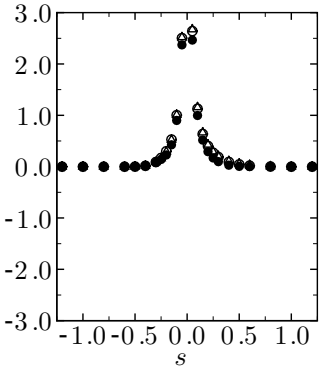

(c) Error in the momentum spike

Figure 6. Normalized error in density and momentum. Filled circles: Roe solver; open circles: Roe solver with fix;[8] open triangles: HLL solver with current fix.

not significantly damped by the numerical viscosity away from the shock. Thus, the numerical errors persist, propagate in the entire flow field and may interact with physical flow features. As illustrated by Figure 7, the wavelength of the error decreases and its amplitude increases. This behavior may be understood by writing the flux difference for Lax-Friedrichs as a high-order accurate central difference, followed by a diffusive term:

$$\frac{f_{i+1/2} - f_{i-1/2}}{\Delta x} = \frac{\frac{f^R_{i+1/2}+f^L_{i+1/2}}{2} - \frac{f^R_{i-1/2}+f^L_{i-1/2}}{2}}{\Delta x} - \frac{\alpha \Delta z}{2} \frac{\frac{q^R_{i+1/2}-q^L_{i+1/2}}{\Delta z} - \frac{q^R_{i-1/2}-q^L_{i-1/2}}{\Delta z}}{\Delta x}, \tag{30}$$

where Δz is some spacing that is expect to vary with $q^R_{i+1/2} - q^L_{i+1/2}$.

The diffusive term consists of a low-order accurate approximation of high-order accurate first derivative in the diffusion term. As the order of accuracy increases, the difference between $q^R_{i+1/2}$ and $q^L_{i+1/2}$ becomes smaller, so that Δz is smaller as the order of accuracy is increased. In other words, the artificial viscosity coefficient decreases with increasing order of accuracy, thus preventing an appropriate amount of dissipation to be generated near the shock and leading to overshoots and undershoots.

To correct this behavior, different approximations for the numerical flux in terms of a central difference term and an artificial viscosity term are considered:

1. $f_{i+1/2} = \frac{f^L_{i+1/2}+f^R_{i+1/2}}{2} - \frac{\alpha}{2}(q^R_{i+1/2} - q^L_{i+1/2})$
2. $f_{\mathrm{i}+1/2} = \frac{f^L_{i+1/2}+f^R_{i+1/2}}{2} - \frac{\alpha}{2}(q_{i+1} - q_i)$

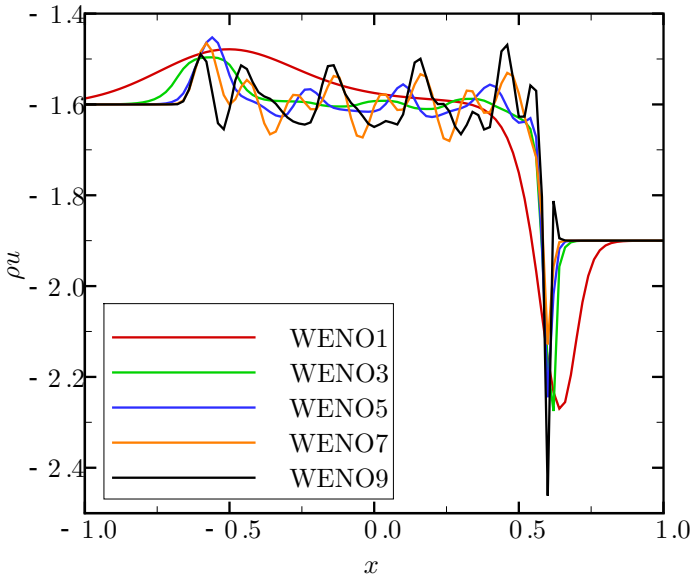

Figure 7. Momentum profiles for $s = 0.1$, using the Lax-Friedrichs solver for different orders of accuracy.

3. $f_{i+1/2} = \frac{f^L_{i+1/2}+f^R_{i+1/2}}{2} - \frac{\lambda^{(2)}_R}{2}(q^R_{i+1/2} - q^L_{i+1/2})$

4. $f_{i+1/2} = \frac{f^L_{i+1/2}+f^R_{i+1/2}}{2} - \frac{\lambda^{(2)}_R}{2}(q_{i+1} - q_i)$

The first definition is the original numerical flux used in WENO with a Lax-Friedrichs solver. In the second and fourth definitions, the diffusive term consists of a central difference term. In the third and fourth definitions, the artificial viscosity coefficient is modified. As shown in Figure 8, the fourth option yields the smallest oscillations (but with the most dissipation). If the goal is to prevent oscillations, the fourth definition is the preferred one. However, it only needs to be applied near slowly moving shocks, which can be detected as described in Section VI.

VIII. Extension to the Euler equations

The extension of the present HLL and high-order accurate fixes to the Euler equations and multi-dimensions is trivial. As an example, the two-dimensional interaction of a slowly moving shock with an entropy wave is considered in Figures 9 and 10 for Roe's scheme with fifth-order accurate WENO and for the proposed fix with the modified fifth-order accurate WENO scheme. It is clear that Roe's scheme leads to significant oscillations in the density and momentum downstream. These oscillations are so severe and die out so slowly that the entropy wave and the waves generated upon the interaction with the shock are barely discernible. On the other hand, the proposed scheme leads to smooth solution, although at the expense of additional dissipation at the shock.

Similar errors have been observed in the interaction of a vorticity wave with a shock.[7] However, in this problem, errors appeared to be dependent on the angle of the vorticity, and not only on the shock speed.

IX. Conclusions

The errors generated by shocks moving slowly compared to the grid are analyzed in the present work. The errors are divided into two classes: *start-up* errors and *post-shock oscillations*. It is shown that a traveling wave analysis[6] describes the spike formation in the momentum for the Lax-Friedrichs solver very well. By smearing the density and momentum profiles appropriately, the corresponding downstream-propagating wave can be removed. The post-shock oscillations have been characterized; as a fix for this problem, a lower bound on the wave speed of the HLL solver is set in the artificial viscosity coefficient for density in the continuity equation. The implementation to higher-order accurate methods is not straightforward; an additional fix

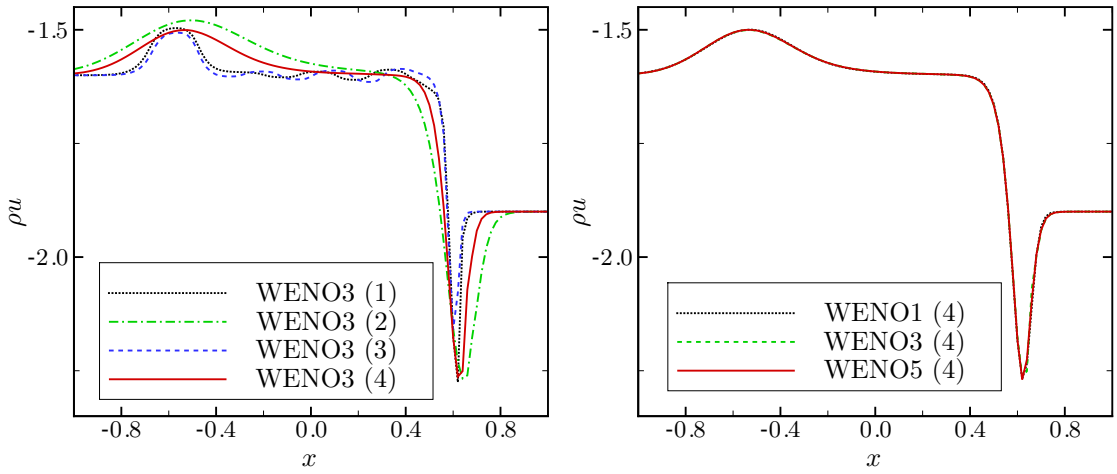

Figure 8. Momentum profiles for $s = 0.1$, using the Lax-Friedrichs solver for different expressions of the numerical flux defined in the text.

is proposed, in which the flux difference is written in terms of central difference and numerical diffusion components. The fixes are local, in that they need not be applied in the entire flow field, and have been tested on a variety of problems, including the full Euler equations in multiple dimensions. Future work includes studies of interactions between slowly moving shocks and more complex flow features.

Acknowledgments

The authors wish to thank S. Kawai for useful discussions. This work was supported by DOE-SciDAC (Grant DE-FC02-06-ER25787).

References

[1]Arora, M., Shariff, K., 1997. On postshock oscillations due to shock capturing schemes in unsteady flows. J. Comput. Phys. 127, 27–51.

[2]Colella, P., Woodward, P. R., 1984. The piecewise parabolic method (PPM) for gas-dynamical simulations. J. Comput. Phys. 54, 174–201.

[3]Gottlieb, S., Shu, C. W., 1998. Total-variation-diminishing Runge Kutta schemes. Math. Comp. 67, 73–85.

[4]Harten, A., Lax, P. D., van Leer, B., 1983. On upstream differencing and Godunov-type schemes for hyperbolic conservation laws, SIAM Rev., 25, 35–61.

[5]Jiang J. S., Shu, C. W., 1996. Efficient implementation of weighted ENO schemes, J. Comput. Phys. 126, 202–228.

[6]Jin, S., Liu, J. G., 1996. The effects of numerical viscosities. I. Slowly moving shocks. J. Comput. Phys. 126, 373–389.

[7]Johnsen, E., Larsson, J., Bhagatwala, A. V., Cabot, W. H., Moin, P., Olson, B. J., Rawat, P. S., Shankar, S. K., Sjogreen, B., Yee, H. C., Zhong, X., Lele, S. K., 2010. Assessment of high-resolution methods for numerical simulations of compressible turbulence. J. Comput. Phys. 228, 1213–1237.

[8]Karni, S., Canic, S., 1997. Computations of slowly moving shocks. J. Comput. Phys. 136, 132–139.

[9]Lax, P. D., 1954. Weak solution of nonlinear hyperbolic equations and their numerical approximation. Comm. Pure and Appl. Math. 7, 159–193.

[10]LeVeque, R. J., 2002. Finite Volume Methods for Hyperbolic Problems. Cambridge, UK: Cambridge University Press.

[11]Lin, H. C., 1995. Dissipation additions to flux-difference splitting. J. Comput. Phys. 117, 20–27.

[12]Quirk, J. J., 1994. A contribution to the great Riemann solver debate. Int. J. Numer. Methods Fluids 18, 555–574.

[13]Roberts, T. W., 1990. The behavior of flux difference splitting schemes near slowly moving shock waves. J. Comput. Phys. 90, 141–160.

[14]Roe, P. L., 1981. Approximate Riemann solvers, parameter vectors, and difference schemes. J. Comput. Phys. 43, 357–372.

[15]Rusanov, V. V., 1961. Calculation of interaction of non-steady shock waves with obstacles. J. Comput. Math. Phys. USSR. 1, 267–279.

[16]Stiriba, Y., Donat, R., 2003. A numerical study of postshock oscillations in slowly moving shock waves. Comput. Math. Appl. 46, 719–739.

[17]Toro, E. F., 1999. Riemann solvers and numerical methods for fluid dynamics. Heidelberg, Germany: Springer-Verlag.

[18]Woodward, P. R., Colella, P., 1984. The numerical simulation of two-dimensional fluid flow with strong shocks. J. Comput. Phys. 54, 115–173.

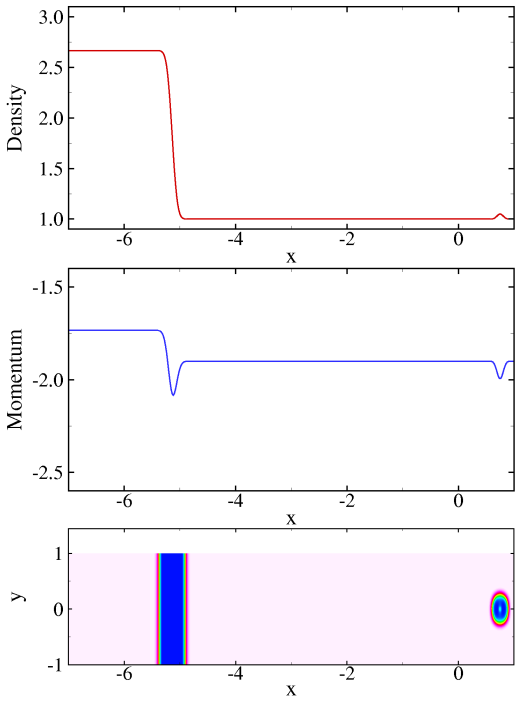

Figure 9. Two-dimensional interaction of a slowly moving shock with an entropy wave (initial conditions). Top: density profile along the centerline; middle: momentum profile along the centerline; bottom: numerical Schlieren contours.

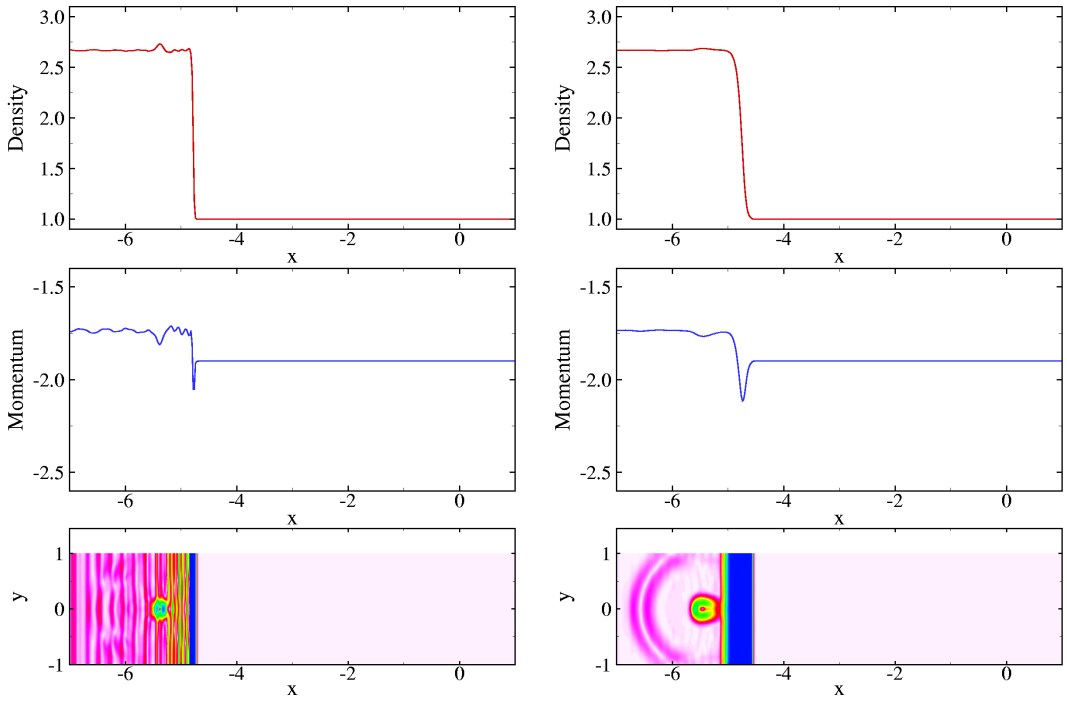

(a) Roe's scheme with WENO5. (b) Proposed scheme with modified WENO5.

Figure 10. Two-dimensional interaction of a slowly moving shock with an entropy wave (just after interaction with shock). Top: density profile along the centerline; middle: momentum profile along the centerline; bottom: numerical Schlieren contours.